Scientific Reports

https://doi.org/10.1038/s41598-026-41147-5

Article in Press

MALDI-TOF mass spectrometry imaging of sulfatide lipid expression in the CNS of mice with experimental autoimmune encephalomyelitis

Received: 7 October 2025

Accepted: 18 February 2026

Published online: 28 February 2026

Cite this article as: Berlin K.A., Huizar C.C., Garza C. *et al.* MALDI-TOF mass spectrometry imaging of sulfatide lipid expression in the CNS of mice with experimental autoimmune encephalomyelitis. *Sci Rep* (2026). https://doi.org/10.1038/s41598-026-41147-5

Krista A. Berlin, Carol Chase Huizar, Celeste Garza, Thomas G. Forsthuber & Stephan B. H. Bach

MALDI-TOF mass spectrometry imaging of sulfatide lipid expression in the CNS of mice with experimental autoimmune encephalomyelitis

Krista A. Berlin[1], Carol Chase Huizar[2], Celeste Garza[2], Thomas G. Forsthuber[2,3], Stephan B. H. Bach[1,3*]

1 Department of Chemistry, the University of Texas at San Antonio, San Antonio, Texas

2 Department of Molecular Microbiology and Immunology, the University of Texas at San Antonio, San Antonio, Texas

3 Contributing Authors

Abstract: Changes in the composition and distribution of the lipids comprising the myelin sheath surrounding neuronal axons have been under-explored in neuroinflammatory diseases such as multiple sclerosis due to the complexities in the analysis of lipids in biological tissues. The application of mass spectrometry-based molecular imaging enables the study of the molecular components of demyelinating tissue. This provides a much better understanding of the complex molecular processes involved in lipid metabolism and the underlying neuroinflammatory demyelinating processes. Uncovering alterations in the lipid profiles during the demyelination processes can potentially elucidate new molecular targets for novel MS drug therapies.

We have utilized mass spectrometry imaging (MSI) of in-situ sulfatide lipids in mouse CNS tissue to reveal their spatial distribution and relative abundance. We show that they are generally confined to the white matter region of the cerebellum. We provide a molecular snapshot of lipid alterations at different disease stages of experimental autoimmune encephalomyelitis (EAE), the animal model for MS. Our results suggest that alterations in sulfatide expression are greatest prior to the onset of clinical disease symptoms and are systemic through the white matter and not restricted to the focal inflammatory lesions pathognomonic of EAE and human MS. The lipid mass maps generated by MSI provide novel insights into the dynamics of lipid alterations during neuroinflammation.

Key Words: *mass spectrometry imaging, lipid imaging, neuroinflammation, EAE, CNS, multiple sclerosis*

Introduction: Multiple sclerosis (MS) is the most frequent neuroinflammatory autoimmune disease of the central nervous system (CNS), impacting millions of people worldwide. It is the most commonly diagnosed complex degenerative brain disease in young adults[1]. While the pathology and etiology of MS have yet to be fully resolved, advancements in understanding the autoimmune response have led to several FDA-approved disease-modifying therapies (DMTs) that are effective at treating the most common form of MS, relapsing-remitting multiple sclerosis (RRMS)[2]. A deeper understanding of the molecular components involved in the disease's pathophysiology, especially myelin-specific lipids, is critical for investigating and developing a better understanding of the pathology and etiology of disease progression and exploring alternative DMT targets.

The presence of focal areas of neuroinflammation-mediated demyelination within the brain and spinal cord white matter is a histopathological hallmark of MS[1]. The myelin sheaths surround neuronal axons and act as an insulator, aiding in the conduction of neuronal electrical signaling while also providing metabolic support for axon function[3]. Myelin sheaths are formed by large dendritic-like extensions of the oligodendrocyte plasma membrane within the CNS that spirally wrap around axons[4,5]. Myelin sheaths exhibit a complex, multilamellar membrane structure containing highly heterogeneous functional and structural molecular domains[6]. Since axon insulation is a major responsibility of myelin, it is predictably rich in lipids, making up 73-81% of total myelin content by dry weight[7].

During neuroinflammatory disease, the inflammatory events cause CNS tissue damage characterized by demyelination and axonal transection. As inflammatory demyelination progresses, it results in the build-up of cellular debris and lipid-laden macrophages detrimental to remyelination[8,9]. Previous studies found increased levels of myelin debris in the cerebrospinal fluid (CSF) of MS patients, including myelin-specific lipids such as sulfatides. Furthermore, studies showed altered levels of phospholipids, sphingolipids, and ceramides in the CSF of MS patients[10,11]. The accumulation of lipids in the CSF of MS patients indicates that myelin is being broken down at a faster rate than the brain's homeostatic repair mechanisms.

Excluding adipose tissue, myelin has the highest lipid content of any tissue in the body. The profile of the myelin lipid bilayer surrounding axons is dominated by cholesterol and glycolipids, specifically, 3-*O*-sulfogalactosylceramide (sulfatide) and its metabolic precursor, galactosylceramide (GalCer)[6]. This composition is unique to myelin and significantly higher than in any other tissue[12]. Sulfatides are linked to pertinent cellular processes within myelin and its molecular construction, making investigating neuronal sulfatides a promising initial step in understanding the dynamics of lipid perturbations during neuroinflammation.

Sulfatide, the most abundant sulfoglycolipid in the human brain, was first isolated in the late 1800s[13]. Since its initial description, researchers have associated sulfatide and its precursor, GalCer, with structural and functional properties of the myelin sheath and regulation of oligodendrocyte maturation, maintenance, and myelin formation[6,14,15]. Depending on the tissue type and function, sulfatides exhibit various molecular structures, including different acyl chain lengths and ceramide moieties. Neuronal sulfatides typically exhibit an 18-carbon-chain-length amino alcohol sphingoid base, sphingosine, and are accompanied by a 16 to 24-carbon-

chain-length ceramide moiety, with or without hydroxylation (Supplemental Figure S1). The sulfatides within more mature CNSs exhibit predominantly longer carbon chain lengths[16]. Table 1 lists some relevant reported neuronal sulfatides compiled from available literature and cross-referenced with Lipid Maps.

Myelin sulfatides have been associated with many glial membrane functions, including negative regulation of oligodendrocyte differentiation, inhibition of myelin-associated axon outgrowth, and mediation of glial-axon signaling via Na^+/K^+ ion channel clusters[12,14,15,17]. Abnormal sulfatide metabolism has been linked to neurodegenerative diseases such as Alzheimer's disease and metachromatic leukodystrophy, as well as MS[18,19]. The abnormally high ratios of glycolipids within myelin and the metabolic alterations in sulfatide production associated with neurologic disorders make sulfatide lipids a relevant starting point for investigating lipid profiles during disease development and progression.

Using mass spectrometry to investigate lipids poses substantial challenges. Lipids are isomeric and isobaric in nature, making the identification of individual species challenging. In addition, lipids are typically hydrophobic, limiting their solubility in aqueous solutions. Advancements in mass spectrometry have helped overcome these hurdles and provide the foundation for investigating changes in lipid composition during CNS neuroinflammation.

The earliest mass spectrometric studies of MS have focused primarily on proteomic profiling of bodily fluids, including serum, urine, saliva, and tears, as well as the CSF of patients at different disease stages[20-25]. Nonetheless, previous liquid chromatography coupled to mass spectrometry (LC-MS) and matrix assisted laser desorption ionization time-of-flight (MALDI-TOF) mass spectrometry studies were limited to fluids and homogenized tissue samples. Homogenization of tissues for lipid or protein extraction and subsequent LC-MS/MS analysis eliminates molecular spatial information. This removes critical topological and morphological information about the tissue distribution of the respective lipids/proteins[26]. However, this information is vital for understanding the structure-function relationship between cells (e.g., neurons, microglia, and inflammatory cells) and tissue components such as lipids.

Mass spectrometry imaging (MSI) using MALDI-TOF mass spectrometry is an analytical technique that allows for the simultaneous analysis of hundreds of biomolecules in situ while preserving tissue architecture and the location of the molecules in the tissue. This preserves the critical structure-function information[26-29]. MALDI-TOF MSI is a label-free, two-dimensional molecular imaging technique with < 20 µm spatial resolution

capable of generating mass maps of the molecules residing within tissues. This methodology provides visualization of the analytes' molecular spatial distribution, colocalization, and relative abundance. Furthermore, MSI can correlate molecular changes in the tissue structures with corresponding histological images and provide a molecular snapshot of the metabolic state of tissues[30,31]. It is a unique and powerful approach to elucidate the small molecules and metabolites present in tissue that are not readily detected by traditional imaging methods, such as microscopy.

Previous studies sought to profile the proteome of myelinated and demyelinated regions of postmortem brain lesions of MS patients and murine brains, but investigations of MALDI-TOF MSI for lipid profiling are limited[29,32-34]. A MSI lipid study of Alzheimer's patients' brains examined the molecular distribution of hydroxylated versus non-hydroxylated sulfatides within the human cerebral cortex. The authors reported higher concentrations of hydroxylated sulfatides expressed in oligodendrocytes within grey matter and a reversal of the ratios of higher versus non-hydroxylated sulfatides along the border with white matter[35]. Other MSI studies have correlated various lipids and peptides to region-specific amyloid plaques of transgenic mice[19,36]. Fletcher and coworkers have investigated the myelin loss observed with amyloid in specific regions of the murine brain[37]. A recent study has reported lipid dysregulation in L-DOPA induced dyskinesia using a primate model of Parkinson's disease[38]. They investigated three specific regions of the macaque brain, the pallidus intern, claustrum and the precentral gyrus. MSI lipid profiling has also been employed to investigate cardiolipins in retinal cell layers, chronic cerebral hypoperfusion lipid dynamics, and ganglioside and ceramide localization during Niemann-Pick disease[39]. However, there is a lack of studies investigating lipid profiles during neuroinflammation in MS or its animal models. We posit that elucidating the spatial distribution and relative abundance of myelin sulfatides will provide novel mechanistic insights into the dynamics and role of sulfatides in the demyelination process and disease progression.

Preclinical animal models of human MS are valuable tools for investigating its pathogenic mechanisms. Experimental autoimmune encephalomyelitis (EAE) models show many similarities to MS, including CNS inflammation, demyelination, axonal damage, and gliosis. EAE is considered the gold standard for studying MS[40,41]. This study utilizes MALDI-TOF MSI to investigate specific myelin lipids in a preclinical adoptive transfer EAE model. The goal is to provide novel insights into lipid alterations during neuroinflammatory demyelination.

Results and Discussion

We examined the utility of MSI to investigate lipid profiles of select CNS myelin lipids (Table 1) in the healthy murine brain as well as during

neuroinflammation using the EAE model. The goal was to gain novel insights into their morphological distribution. Specifically, the studies interrogated the co-localization, spatial distribution, and relative abundance of selected sulfatide lipids. Because of the untargeted nature that MSI is capable of, we also examined untargeted lipids from various lipid classes that were observed.

It is important to establish a robust sample preparation method for investigating lipids in brain tissue, which is notoriously difficult. A key obstacle for mass spectrometry is achieving proper ionization of analytes within a sample. Isolating or detecting low-abundance analytes can be challenging in complex biological samples using MSI. The state of the sample and the analytes of interest will directly impact sample preparation.

Lipid ionization is driven by the lipid's functionality or headgroup[42,43]. Thus, we optimized the sample preparation for this study to target the sulfatide class lipids. The 3-*O*-sulfated galactosyl of the sphingolipid base causes the sulfatide lipids to preferentially ionize in negative ionization mode. The sulfatides selected for this study have a mass range of approximately 800 - 925 Da (Table 1). The low mass range of sulfatide lipids can render them susceptible to matrix interference and undesired fragmentation. Thus, 9-aminoacradine (9-AA) was chosen to yield the best analyte signal for the MSI of in situ neuronal sulfatides. This was based on literature review and preliminary studies (see Supplemental Figure S2)[44,45].

Table 1. Select Neuronal Sulfatides

Sulfatide Lipid Species (SHexCer)	Precursor Ion (m/z) [M-H]-
SHexCer 36:1;O2	806.62
*SHexCer 36:1;O3	822.60
SHexCer 38:1;O2	834.57
*SHexCer 38:1;O3	850.55
SHexCer 40:1;O2	862.60
*SHexCer 40:1;O3	878.58
SHexCer 42:2;O2	888.65
SHexCer 42:1;O2	890.62
SHexCer 42:2;O3	904.63
SHexCer42:1;O3	906.60

All contain an 18:1 sphingosine sphingoid base with a varying carbon chain ceramide moiety, with or without hydroxylation of the ceramide chain
* denotes hydroxylated species

To avoid interference from the polymers in the optimal cutting temperature (OCT) compound typically used for cryosectioning tissues, tissues were molded in gelatin. Since the cerebellum of the brain is the region where EAE lesions are frequently observed, we focused on this area[40].

MALDI-TOF MSI of sulfatides replicates tissue morphology: Illustrated in Figure 1A is the spatial orientation and location of the cerebellum within the tissue samples. Figure 1B shows a representative example of a scanned image of the cerebellum of a naïve tissue sample prior to matrix application. Figure 1C shows the same tissue section after MALDI MSI and after histological staining by H&E. MALDI MSI maintains the structural integrity of the tissues. This enables the subsequent histological staining by H&E. The cellular layers of the cerebellum remain preserved as indicated by the arrows in Figure 1C. Therefore, the H&E-stained cerebellum structures can be correlated to the MALDI MSI-generated images in Figure 1D to provide information on spatial distribution of lipids.

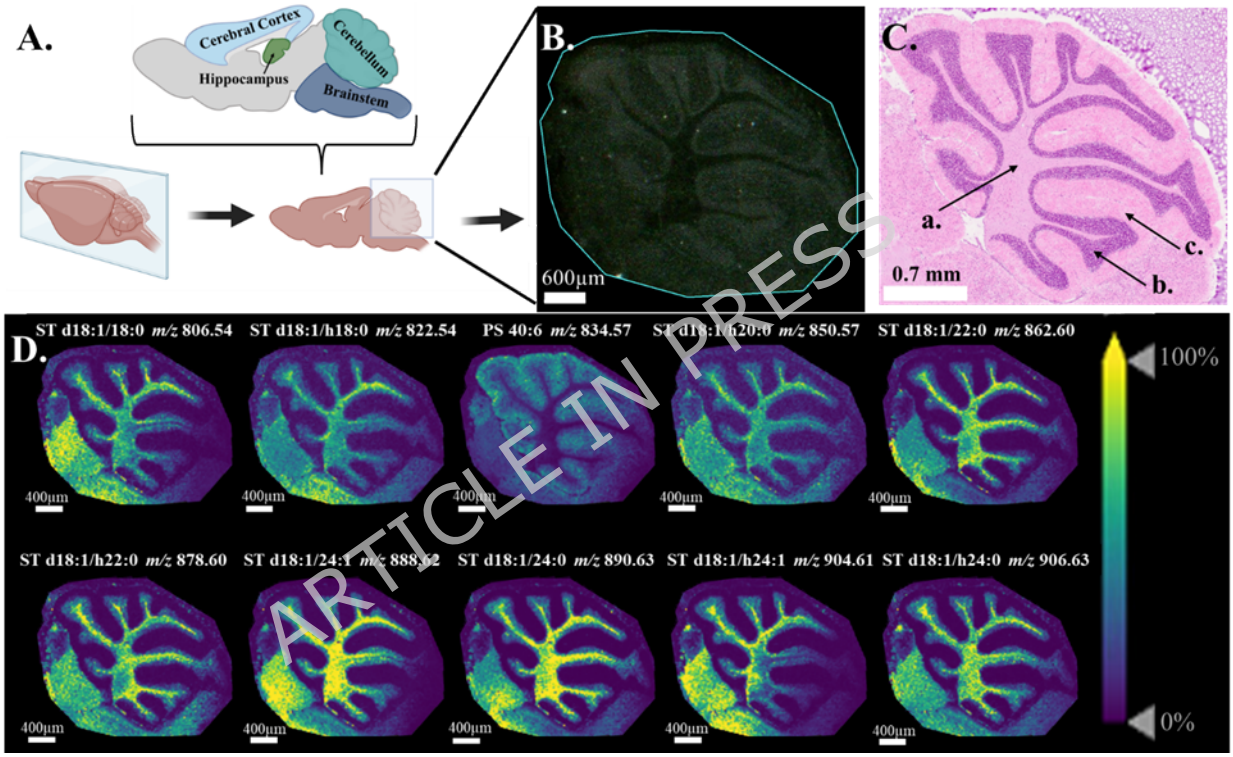

Figure 1. MALDI-TOF MSI mapping of sulfatides in the cerebellum. Shown in (A) is an illustration of tissue orientation for MSI. (B) is a representative scanned image of a tissue section prior to matrix application used for instrument teaching (600 µm scale-bar). Shown in (C) is the H&E-stained tissue after MSI was performed and the matrix washed off. (0.7 mm scale-bar). Indicated by the arrows are (a.) the white matter of the cerebellum, (b.) the granule cell layer, and (c.) the molecular layer or gray matter. Shown in (D) are the MALDI-TOF MSI mapping of ten neuronal lipids within the tissue (400 µm scale-bar). MSI data was collected in the negative ion mode, and TIC was applied for data normalization. The color scale correlates to ion intensity (dark blue = little to no signal and yellow = strongest signal).

Of the selected sulfatides in Table 1, nine co-localized to the white matter tracts of the cerebellum. The exception was the *m/z* 834.57 Da ion. This was anticipated to be the SHexCer 38:1;O2 sulfatide. The *m/z* 834.57 Da ion appeared to be more strongly localized to the grey matter of the cerebral tissue rather than the white matter. Due to the isomeric and isobaric nature of lipids, orthogonal expression (grey vs. white matter) of ions containing the similar *m/z* values can be problematic. PS 40:6 and PE 44:12, both nitrogen-containing phospholipids, preferentially ionize in negative mode and have ion expressions orthogonal to the SHexCer 38:1;O2 sulfatide[46]. Lipids possessing orthogonal ion distributions matching that of the sulfatides in our study were reported to reside in alternate structures of the cerebellum[46-49].

To confirm the identification of the selected sulfatide lipids, we investigated serial sections of naïve samples and generated diagnostic fragmentation profiles by MALDI TOF MS/MS (work done at the UT Austin Mass Spectrometry Imaging facility). The fragmentation profiles of the lipids were uploaded to Metaboscape 2024 (Bruker Daltonics, Billerica, MA) for lipid annotation and cross-referenced with LIPID MAPS Structure Database (LMSD) for punitive identification (Supplemental Figures S4A-J for annotated MALDI-TOF MS/MS spectra). The MALDI-TOF MS/MS data resulted in confirming the identification, using fragmentation profiles, for nine of the ten sulfatide lipids. The *m/z* 834.57 ion, primarily localized to the grey matter of the cerebellum, was identified as PS 40:6 (Supplemental Figure S4C) using accurate mass and fragmentation profiles.

Lipid profile alterations manifest prior to obvious clinical signs of EAE. To investigate whether and when alterations in lipid expression could be detected at different stages of the disease course, we induced passive EAE in C57BL/6 female mice by adoptive transfer of MOG_{35-55} reactive T cells as previously described[50]. In this protocol, EAE manifests as the monophasic disease. The lipid profiles were evaluated by MSI at three pre-determined stages and compared with age-matched naive control mice (Table 2).

Table 2. EAE Clinical Disease Scoring

EAE Score	Neurological Deficit	Disease Phase*	Observed Number of Days after Adoptive Transfer*
0	No clinical disease	Pre-Onset	8
1	Flaccid tail	Onset	13
2	Partial hind-limb paralysis		

3	Total hind-limb paralysis	Peak	18
4	Front and hind-limb paralysis		
5	Moribund or dead		
* n=3 for all time points and each time point is accompanied by an age-matched naïve mouse as control. Time points were determined by the clinical score.			

Using SCiLS software (Bruker Daltonics, Billerica, MA), regions of interest (ROIs) were defined by tracing each scanned tissue sample's white matter and grey matter using the post-MSI H&E-stained tissue for guidance. Figure 2 shows the scanned tissue images with the defined white matter ROI overlaid. ROI were color-coded and encircled by disease phase and the sample from the control animal. TIC normalization was applied to all MSI data sets before grouping. Comparison of the naïve MSI ion distributions to the MSI ion distributions of the three disease phases indicates that the sulfatide lipid class generally maintain white matter co-localization. Examination of the overlaid average spectra of the respective sulfatides revealed notable variations for some of the lipids between the EAE and naïve samples between the disease stages as indicated by the colored coded mass spectra (Figure 3). In particular, SHexCer42:2;02 was markedly altered between the different time points, whereas some of the lipids remained essentially unchanged in their relative expression (Figure 3). White matter ion distribution is shown in supplemental Figure S5D.

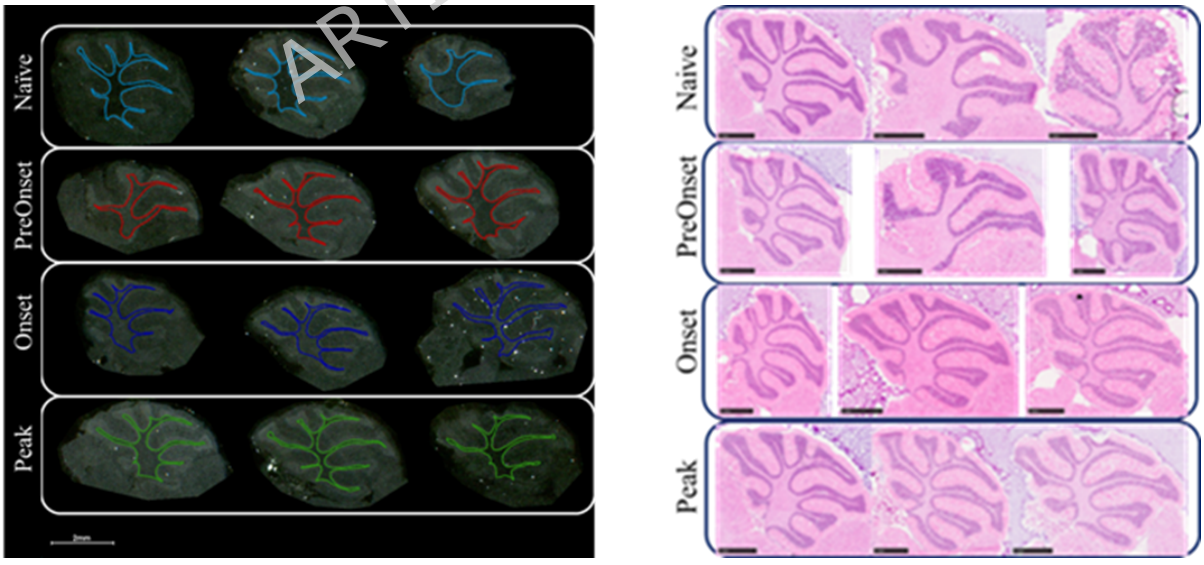

Figure 2. Shown are the WM regions and the corresponding H&E stained tissue post-MSI. Layout of the samples is grouped by observed disease phase with the naïve group in the top row.

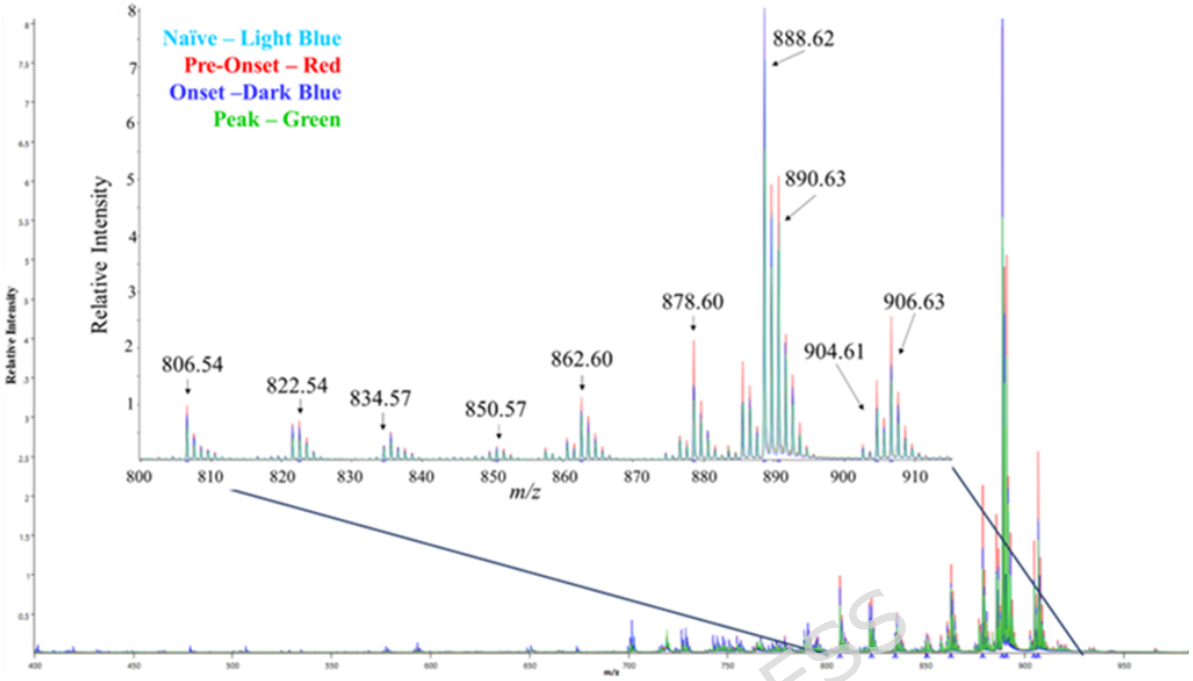

Figure 3. Comparison of the average mass spectra of the 4 states, naïve (light blue), pre-onset (red), onset (dark blue) and peak (green).

The graphical analysis of the average relative intensity of each disease stage and the naïve control suggests fluctuations within the EAE sulfatide lipid profile before outward signs of the disease became apparent (SHexCer42:2;02; red vs blue; Figure 4). The pre-onset disease stage showed elevated expression of the SHexCer 36:1;O2 (*m/z* 806.62), SHexCer 40:1;O2 (*m/z* 862.60), SHexCer 40:1;O3 (*m/z* 878.58), and SHexCer 42:1;O3 (*m/z* 906.60) (Figure 4). The MSI ion intensity maps for the 4 sulfatides with an increase in average intensity in the pre-onset phase are shown in Figure 5. Decreased expression of SHexCer 42:2;O2 (*m/z* 888.62) was also observed (Figure 4)[51,52]. Even minor variations in lipid abundance and the mis-metabolism of lipids may potentially interfere with proper synaptic function[3,18,53].

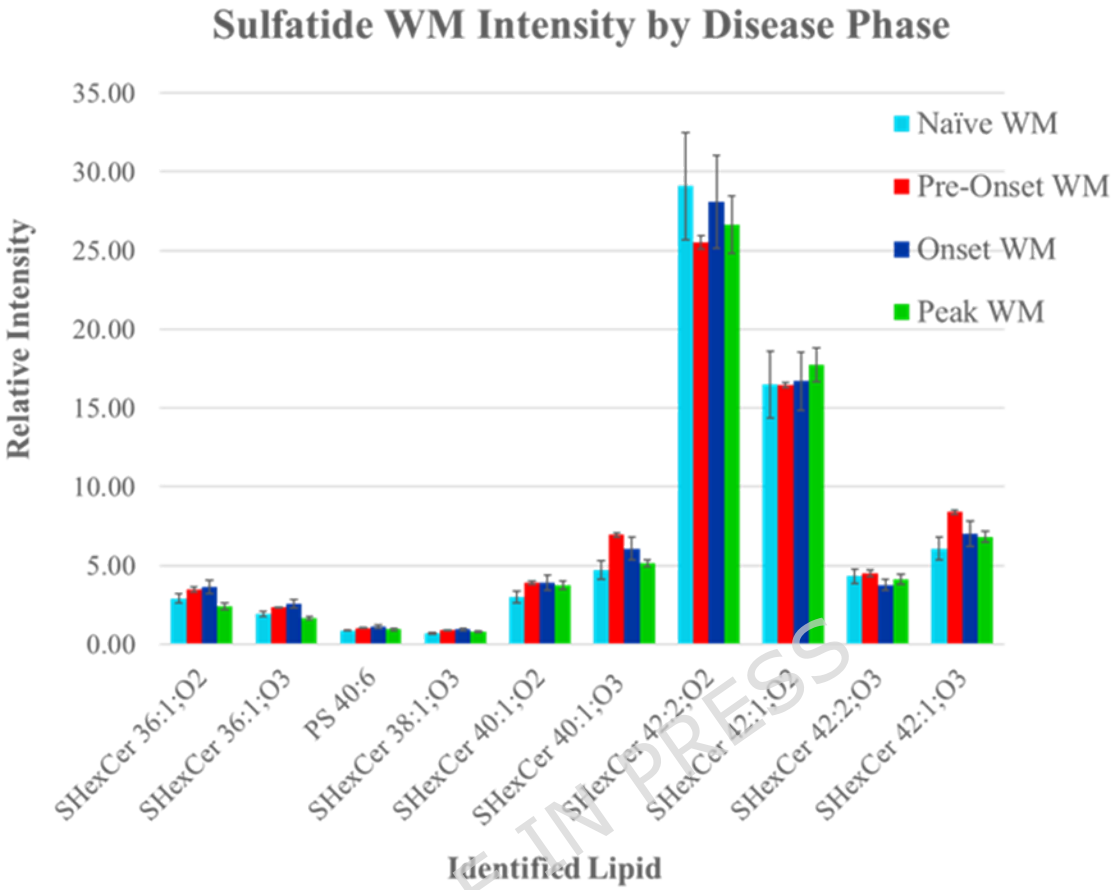

Figure 4. Graphical representation of the average ion intensity for each disease phase and naïve for all 10 of the selected lipids. Individual error bars were calculated using the standard error of the mean (SEM).

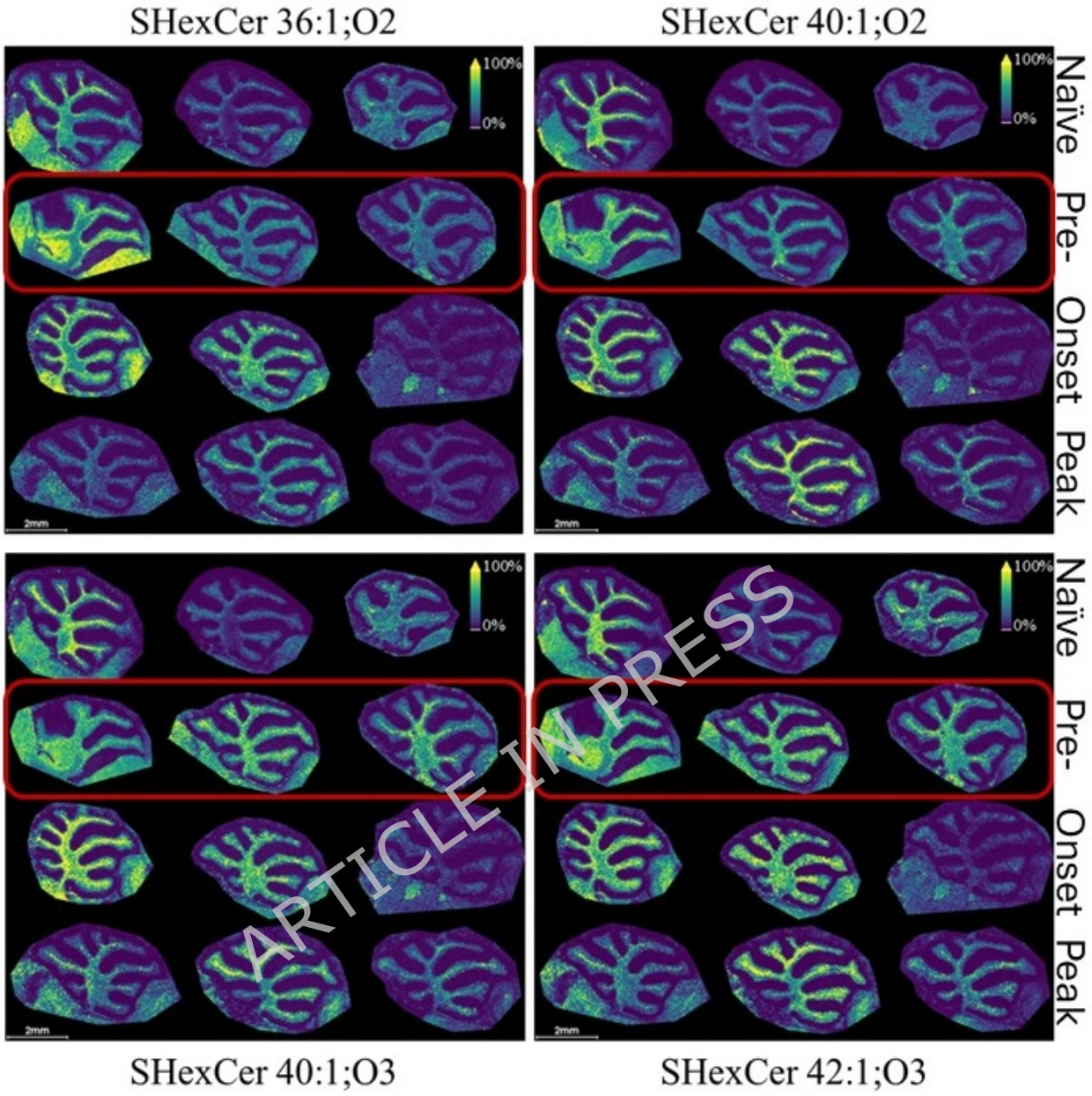

Figure 5. The MSI ion distribution of the 4 sulfatides with an increase in average intensity in the pre-onset disease phase (encircled in red and labeled Pre-). The top row is the Naïve stage, the third row is the Onset stage and the bottom row is the Peak stage. All images have a 2 mm scale bar (lower left) and a mass window of ±0.2 Da. MSI data was collected in negative ion mode and TIC was applies for data normalization. The color scale correlates to ion intensity (dark blue = little or no signal, yellow = strongest signal.

To gain further insights into sulfatide expression at different disease stages, principal component analysis (PCA) was performed on the whole cerebellum

of all samples and grouped by disease stage and naïve. The PCA plots used the feature list option using the 10 lipids listed in Table 1. Shown in Figure 6 A-D is the PCA for each group (naïve (light blue), pre-onset (red), onset (dark blue), and peak (green) with the grey background being the combined footprint of components one and two, and 95% ellipses. Each point on the scores plot represents the average mass spectra of a MSI pixel. Notably, the PCA of the onset disease phase in Figure 6C reveals a significant divergence from the other three groups. Furthermore, the altered component distribution within the scores plot of the onset disease phase appears to expand equally in opposing component directions. However, the PCA of the peak disease phase seems to return to a component distribution similar to the naïve and pre-onset PCAs. Figure 7 A and B display the PCA of the grey matter and white matter regions. The PCA plots show a significant change in differential component distribution between the two regions. The PCA results support that the lipid profile from neuroinflammation during EAE disease progression changes with disease stage and warrants deeper investigation.

(A) Naïve Scores Plot

(B) Preonset Scores Plot

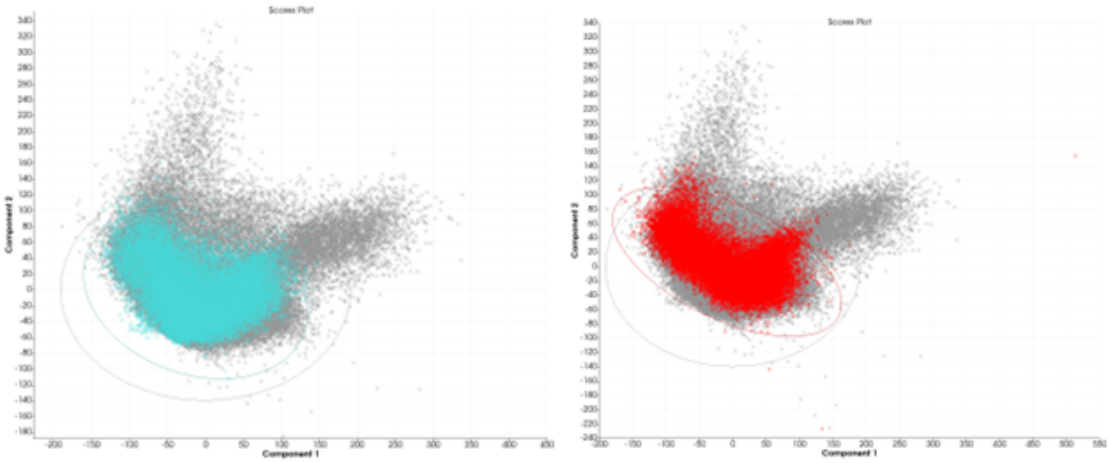

(C) Onset Scores Plot

(D) Peak Scores Plot

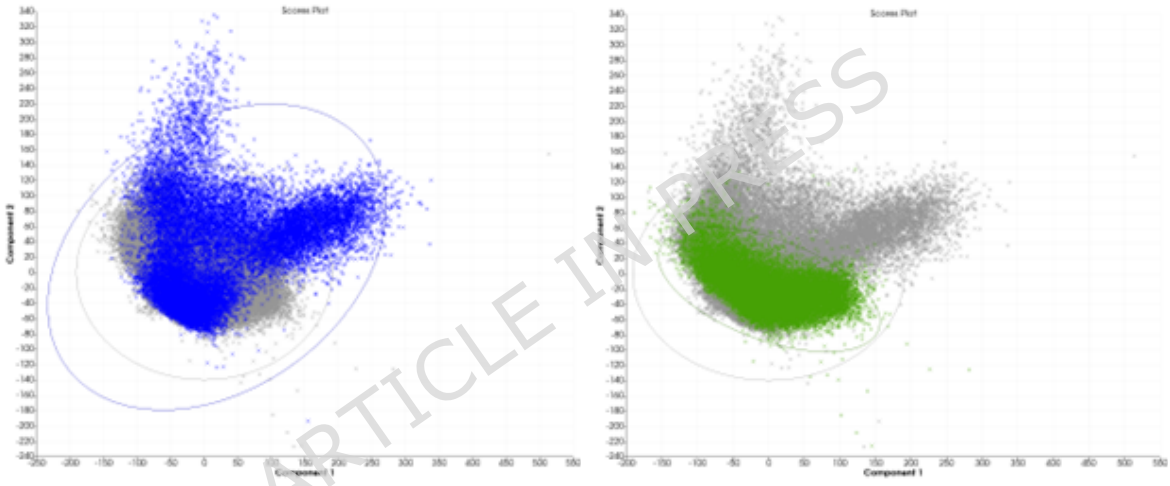

Figure 6. Principle component analyses (PCA) divergence in the onset disease phase.

All disease stages grey matter

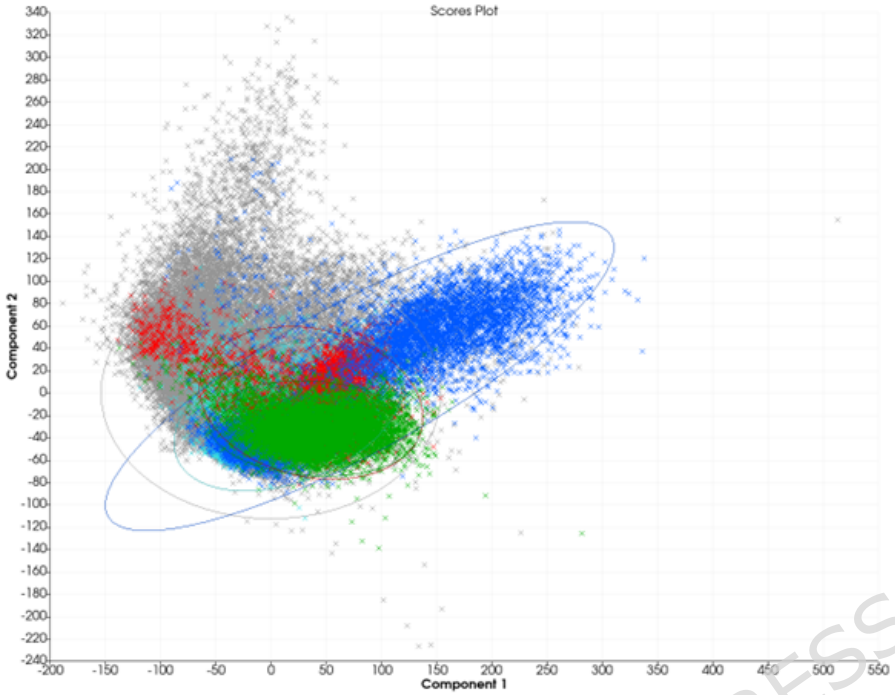

All disease stages white matter

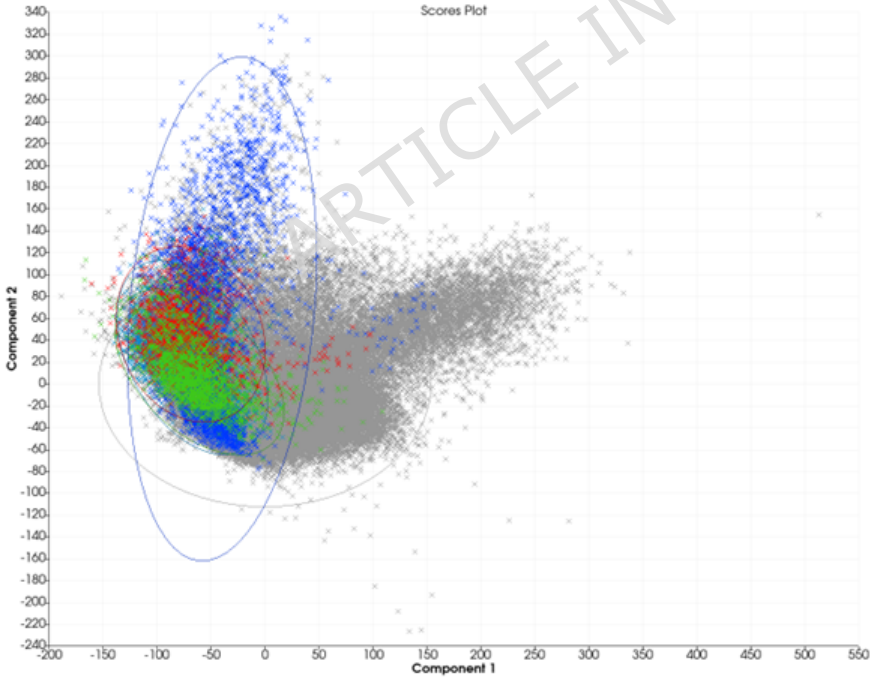

Figure 7. PCA of the GM region and the WM region show differential component profiles between the two defined regions

Our results reveal that alterations in the lipid composition can occur before outward signs of neuroinflammatory disease become apparent (pre-onset). Furthermore, the observable molecular profile changes were seen throughout the cerebellum tract in which they resided.

MSI reveals alterations in untargeted lipids in different EAE phases. The untargeted nature of MALDI-TOF MSI permits detection of other lipids in addition to the selected sulfatide lipids. Accordingly, we noted variations in the expression of several unidentified lipids in EAE mice as compared with naïve animals. Interestingly, these additional lipid ions exhibited specific spatial distributions within the white matter tract of cerebellum versus the grey matter tract. In total, 28 non-sulfatide lipids were mapped to the white matter region of the tissue samples across different EAE disease stages (see Supplemental Figure S6D for all the observed grey matter ion distributions), and 30 lipids in the grey matter region. The highly localized molecular distribution of these lipids suggests a functional role in white matter versus grey matter and warrant further investigations.

Implications: Sulfatides have been associated with the maturation and regulation of oligodendrocytes, the myelin-producing cells of the CNS. Additionally, sulfatides play an essential role in the structural support of the myelin lipid bilayer. Myelin debris impair the remyelination process[6,54]. Thus, altered lipid expression will also affect remyelination. In previous studies, the genes for ceramide galactosyltransferase (CGT) and galactosylcerebroside (GalC), responsible for generating sulfatide precursors and sulfotransferase, were deleted individually in knockout mice to investigate their role for myelin composition and structure. The results showed that myelin formation still occurred, but the integrity of the myelin sheath was notably compromised[55]. Arylsulfatase A (ASA) is the enzyme responsible for downregulating sulfatides. A deficiency in ASA leads to metachromatic leukodystrophy which involves the build-up of neuronal sulfatides, causing demyelination and leading to severe neurological symptoms[56]. Similarly, ASA deficient mice that overexpressed the enzyme galactose-3-*O*-sulfotransferase-1, the enzyme responsible for synthesizing sulfatides, showed build-up of sulfatides due to an excess of sulfatide production resulting in severe neurological dysfunction similar to MLD[56]. Thus, altered expression of neuronal sulfatides as revealed by the present study is consistent with a role in demyelinating diseases. Investigating alterations in the lipid profiles in the CNS during neuroinflammatory diseases may provide novel insights into understanding the pathogenesis of MS and its disease progression.

Conclusions:

To our knowledge, this work represents the first study utilizing MALDI MSI to determine myelin sulfatides in situ in the brain of naïve mice and mice with autoimmune neuroinflammation in the preclinical EAE model. The results show the utility of MALDI MSI for investigating lipid profiles in the CNS and visualization of their spatial distribution, colocalization, and relative abundance. Previously, Yuki et al. observed a trend towards hydroxylated sulfatides residing predominantly in the grey matter and non-hydroxylated sulfatides colocalizing in the white matter of the human cerebral cortex[35]. While the human cerebral cortex is more complex than that of a mouse, our results show a similar preferential distribution of myelin sulfatides, with sulfatides preferentially residing in the white matter regions of the murine cerebellum.

Further, our results show that subtle alterations in CNS lipids can be detected prior to the onset of clinical signs of neuroinflammation and are broader and beyond the focal inflammatory lesions observed during neuroinflammation in EAE and MS. Conceivably, these early changes in lipid expression during neuroinflammation may be harbingers of damage to the myelin sheath and the neurological alterations observed in MS patients. It may be feasible to detect these changes with clinical imaging modalities, for example, by MRI, conceivably with novel contrast agents. Furthermore, detection of these lipid alterations may provide relevant clinical information as to the progression of the disease, for example, in radiologically isolated syndrome or clinically isolated syndrome[57].

Of particular interest are the molecular interplay of myelin-associated glycoproteins (MAG), residing exclusively in the periaxonal space, the myelin-oligodendrocyte glycoprotein (MOG), localized to the myelin sheath and oligodendrocyte cellular surfaces, and myelin’s lipid counterparts. In addition to aiding in structural support, both MAG and MOG proteins have been implicated in cellular signaling and oligodendrocyte maturation[3,46,58]. The sulfatides in this study have also been implicated in the developmental and homeostatic processes of oligodendrocytes, the CNS's myelin-producing cells[6,14,59]. How do the molecular colocalizations of myelin’s lipids and proteins support cellular and tissue homeostasis? Could their structural colocalizations be utilized to sway neuronal homeostasis in tissue injury or disease cases? Can alterations in neuronal molecular profiles be observed during other EAE disease courses? How early in disease progression can profile changes be observed?

Here, we showed the utility of mass spectrometric-based tissue analysis to generate molecular maps of in-situ sulfatides of brain tissue during neuroinflammatory disease in the preclinical EAE model. Determining

changes of specific CNS lipids during different stages of neuroinflammation and disease progression may add to the understanding of neuroinflammatory and neurodegenerative processes in MS and other disease conditions and provide further insights into the events promoting de- and remyelination. Conceivably, this information will reveal new molecular drug targets. Further studies need to be done using LC-MS/MS to better distinguish (quantify) the changes in lipid levels in the tissue as the disease progresses since MSI using MALDI -TOF has limitations in the technique's ability to accurately determine changes in lipid levels.

Methods:

Animal Models: All animal procedures were approved by the University of Texas at San Antonio Institutional Animal Care and Use Committee (protocol no. MU050) and performed in accordance with institutional and national guidelines. Experimental design, sample size determination, randomization, blinding, outcome measures, and statistical methods are reported following the ARRIVE 2.0 Essential 10 guidelines. Three pre-determined neurological time points, defined by clinical disease scores, were evaluated. Passive EAE was induced by adoptive transfer of 30 x 10^6 myelin oligodendrocyte glycoprotein $(MOG)_{35-55}$-primed T cells into groups of female C57BL/6 mice (n = 9/group), three mice per time point. Groups sizes were determined by power calculation with 2-sided t-test using GraphPad Prism 9.0.

Additionally, three age-matched naive mice were utilized as controls, giving a total of 12 mice (Table 2). Three pre-determined points of neurological deficits from EAE disease progression were evaluated – pre-onset, onset, and peak (Table 2). For each time-point we used three EAE mice and one age-matched naïve mouse as a control, totaling 12 mice in the study. To induce passive EAE by adoptive transfer, 6-week-old female C57BL/6 donor mice (The Jackson Laboratory, Bar Harbor, ME) were injected subcutaneously with 200 µg MOG_{35-55} emulsified in complete Freund's adjuvant (CFA)[60]. Splenocytes and draining lymph nodes were collected from donor mice on Day 10, post-immunization, and restimulated with 20 µg/mL MOG_{35-55} for 3 days at 37 °C in RPMI containing 10% fetal bovine serum and L-glutamine in the presence of Th17 culture conditions: 20 ng/mL recombinant mouse IL-23 (BioLegend, San Diego, CA), 10 µg/mL anti-mouse IFN-γ monoclonal antibody (R4-6A2, Bio X Cell, West Lebanon, NH). Recipient mice were injected with 30 x 10^6 cells, i.p., and scored daily for clinical EAE for up to 30 days using the following standard EAE scoring system: 0, no abnormality; 1, limp tail; 2, moderate hind limb weakness; 3, complete hind limb paralysis; 4, quadriplegia or pre-moribund state; 5, death[61]. At the peak time point, mice showed an average EAE score of 3.5, with a clinical score of 3 or above indicating severe neuroinflammation.

Brain tissue was procured at the indicated time points, molded in gelatin, and stored at -80° C.

Reagents: Carboxymethylcellulose sodium salt (CMC) (CAS# 9004-32-4) and gelatin from porcine skin (CAS# 900-70-8), and red phosphorus (CAS# 7723-14-0) were purchased from Sigma Aldrich (St Louis, MO). Ammonium formate was purchased from Fisher Scientific (Waltham, MA, CAS# 540-69-2), and 9-aminoacridine (9-AA) was purchased from Tokyo Chemical Industry (Chuo-ku, Tokyo, CAS# 90-45-9). The sulfatide standard, C24:1 mono-sulfo galactosyl(β) ceramide (d18:1/24:1), was purchased from Avanti Polar Lipids (Alabaster, AL CAS# 1246355-69-0), and H&E Staining Kit from Abcam Laboratories (ab245880).

Tissue Preparation: Upon removal, murine brains were dissected into left and right sagittal sections, molded in gelatin following modified methods reported by Nelson et al., and immediately placed in a -80 °C freezer to be stored until sectioning[62]. Tissue sections were cut at a thickness of 10 µm using a LEICA CM1860 UV cryostat. The sections were thaw-mounted on ITO slides (Delta Technologies, Loveland, CO CB-50IN-S111) and stored under nitrogen in a -80 °C freezer until analysis. Slides were prepared for IMS the day they were to be run on the mass spectrometer. This occurred over about a 2-week period. Care was taken to use the same section location from each of the mouse brains to minimize variation due to the location of the sample in the brain. At the time of analysis, the slide-mounted tissue sections were equilibrated to room temperature and vacuum-dried in a desiccator. For lipid analysis, a single 15-second wash in 50 mM ammonium formate at 4 °C and a pH of ~6.4 was performed following methods reported by Angel et al., and the tissue was vacuum-dried in a desiccator[63]. Before the matrix was applied to the washed tissue sections, images of the tissue-mounted slides were taken using an Epson Perfection V37 flatbed scanner. The scanned images were used to transfer tissue location information to FlexImaging 2.1 software for automated mass spectrometric imaging runs. The slides were run over about a 2 week period and run the day they were prepared with matrix for analysis.

Matrix Application: Matrix deposition was carried out in a sublimation apparatus purchased from Chemglass Life Sciences (CG-3038-1) with a fitting plate diameter of 70 mm. The apparatus was coupled to a rough pump and a digital thermocouple vacuum gauge controller and was placed on a sand bath heated by a hot plate (Thermo Fischer SP195025) following methods reported by Yang and Caprioli[64]. Deposition of the matrix, 9-AA, was carried out via sublimation following modified methods reported by Thomas et al[65]. Slides were secured to the bottom of the glass cold finger of the sublimation apparatus via conductive copper tape. Typically, about 300

mg of the matrix was sublimated under vacuum at 15 mTorr. The cold finger was filled with ice water. Sections were sublimated with 9-AA at 170 °C for 5.5 minutes. Following sublimation, the apparatus was removed from the heat and allowed to continue sublimating for about 45 seconds before gently breaking the vacuum. The sublimation parameters (temperature, pressure, and deposition time) were optimized to maximize the ion signal produced by the lipids. The optimal matrix deposition of 9-AA for the MSI analysis of neuronal sulfatides was determined to be about 115-120 µg cm^{-2}. For control, the sulfatide standard was spotted on the slide, and red phosphorus was used for instrument mass calibration. Slides were vacuum dried in a desiccator before being placed in the instrument for MSI analysis.

MALDI Imaging: All MSI data sets were collected on an UltrafleXtreme MALDI-TOF/TOF mass spectrometer (Bruker Daltonics, Bremen, Germany) in reflectron mode with a range of 400-1000 Da. MSI was conducted in negative ionization mode with either a 20 or 40 µm spatial resolution. Instrumentation parameters and raw data acquisition were managed with FlexControl 3.3 software (Bruker Daltonics). Prior to MSI sample analysis, slides with the tissue samples were prepared with two calibration spots. The mass spectrometer was calibrated with red phosphorus following methods reported by Sládková et al[66]. This was used to calibrate the mass scale and adjust the mass resolution. The second spot was a lipid standard: C24:1 mono-sulfo galactosyl(ß) ceramide (d18:1/24:1) from Avanti Research (part # 860571P-1mg). The standard comes as a powder and was reconstituted in 1 mL of chloroform/methanol (2:1) (v/v)). Following reconstitution, standard was separated into 20 µL aliquots in glass vials, evaporated under a stream of nitrogen, and stored in -20 °C for up to 1 year. 1-2 µL of the lipid standard was spotted on the slide along with a separate spot for the red phosphorus calibrator in an area without tissue and matrix. The TIC from the lipid calibration spot was used to normalize MSI TICs between tissue samples. The pulsed ion extraction setting was optimized and set at 0 ns with ~ a 45-55% laser setting and a global attenuator offset of 70%. The smart beam parameter was set to small. Ion source 1 was held at 25 kV, and ion source 2 was kept at 23.7 kV with the lens at 6.5 kV. Approximately 50 shots/pixel were acquired with a 1 kHz repetition rate Smartbeam II Nd: YAG laser. MALDI image acquisition was done using FlexImaging 2.1 (Bruker Daltonics).

Data Processing: The mass spectral information acquired from FlexImaging was imported into SCiLS Lab MVS 2020b Pro software (http://scils.de/; Bremen, Germany) for preprocessing and visualization. Total Ion Count (TIC) normalization was applied to all MALDI-TOF MSI data sets before generating the average mass spectra of groups. Once normalized, data sets were grouped by time point: naïve, pre-onset, onset,

and peak (n = 3 for each time point). H&E stains of each tissue sample were used to define white matter ROIs. The average spectra from each time point were overlaid and qualitatively evaluated for alterations in lipid ion expression. The datasets used during the current study are available from the corresponding author upon reasonable request.

Lipid Conformation: MSI at a 20 µm spatial resolution for lipid conformation was first performed on a serial section of naïve sample 2 using a Bruker timsTOF flex mass spectrometer. The generated MSI data was used for molecular localization guidance. MS/MS was carried out on the tissue area (of the same tissue section) that correlated to high-intensity ion expression for the precursor ion of interest. Tims-TOF MS/MS data was uploaded to Metaboscape 2024 (Bruker Daltonics: Bremen, Germany) for lipid annotation and cross-referenced with LIPID MAPS Structure Database (LMSD) for punitive identification (See Supplemental Figure S4A-J for annotated MALDI timsTOF MS/MS spectra).

H&E Staining: After MALDI-TOF MSI, the 9-AA was washed off in 3 x 1-minute submersions in 100% IPA with gentle agitation. Slides were set horizontally to dry. The matrix wash was followed by a modified H&E Staining Kit protocol from Abcam Laboratories (ab245880). No deparaffinizing was required as the samples were fresh, frozen, and molded in gelatin. Eosin Y was diluted 1:3 (v/v) with a dilution solution suggested by Abcam SDS for Eosin Y (65% EtOH, 3.8 % IPA, 1% Acetic Acid).

Author Information

Corresponding Authors

Stephan B. H. Bach - Department of Chemistry, The University of Texas at San Antonio, San Antonio, Texas 78249, United States. Email: stephen.bach@utsa.edu

Thomas G. Forsthuber - Department of Molecular Microbiology and Immunology, The University of Texas at San Antonio, San Antonio, Texas 78249, United States. Email: Thomas.forsthuber@utsa.edu

Authors

Carol Chase Huizar - Department of Molecular Microbiology and Immunology, The University of Texas at San Antonio, San Antonio, Texas 78249, United States.

Celeste Garza – Department of Allergy Research, The University of California San Francisco, California 94143, United States

Krista Berlin - Department of Chemistry, the University of Texas at San Antonio, San Antonio, Texas 78249, United States.

Author Contributions

K.A.B.: Conducted all MSI analysis, data processing, figure generation, and manuscript writing and editing. C.C.H. performed all murine immunizations, cell culturing, disease scoring, and tissue acquisition. C.G. assisted with animal monitoring and disease scoring and carried out immunofluorescent staining. T.G.F. conceived the studies and reviewed and edited all manuscript drafts. S.B.H.B. Contributed to the design of the mass spectrometry studies, manuscript editing, and final manuscript review.

Acknowledgement: The authors acknowledge the National Institute on Minority Health and Health Disparities (G12MD007591), the National Science Foundation under CHE-1126708, the grant NS117742 from the National Institute of Health (T.G.F.), and support from the Jesse H. & Mary Jones Gibbs Endowed Chair (T.G.F.). The authors would also like to thank Dr. Erin Seeley, from the UT Mass Spectrometry Imaging center (CPRIT RP190617, JSB), for her mentorship, MSI expertise, and assistance in performing timsTOF MS/MS lipid identification. Thank you to Dr. Grace Samenuk for her cryogenic sectioning assistance, MALDI-TOF MSI guidance, and Dr. Andrea Kelley and Dr. Madeline Colley for their MALDI expertise. Finally, the authors thank the UTSA RISE program for its research funding and professional development support.

REFERENCES CITED

1 Meghrajani, V., Bakre, A., Acharya, S. & Kumar, S. Multiple Sclerosis: Diagnosis and Treatment Management in Allopathy. *Journal of Pharmaceutical Research International* **33**, 1227-1234 (2021). https://doi.org/10.9734/jpri/2021/v33i60B34736

2 Hamidi, V., Couto, E., Ringerike, T. & Klemp, M. *A Multiple Treatment Comparison of Eleven Disease-Modifying Drugs Used for Multiple Sclerosis*. (2017).

3 Saab, A. S. & Nave, K. A. Myelin dynamics: protecting and shaping neuronal functions. *Curr Opin Neurobiol* **47**, 104-112 (2017). https://doi.org/10.1016/j.conb.2017.09.013

4 Beyer, B. A. *et al.* Metabolomics-based discovery of a metabolite that enhances oligodendrocyte maturation. *Nat Chem Biol* **14**, 22-28 (2018). https://doi.org/10.1038/nchembio.2517

5 Schaeren-Wiemers, N., van der Bijl, P. & Schwab, M. E. The UDP-galactose:ceramide galactosyltransferase: expression pattern in oligodendrocytes and Schwann cells during myelination and substrate preference for hydroxyceramide. *J Neurochem* **65**, 2267-2278 (1995). https://doi.org/10.1046/j.1471-4159.1995.65052267.x

6 Grassi, S. *et al.* The Role of 3-O-Sulfogalactosylceramide, Sulfatide, in the Lateral Organization of Myelin Membrane. *Neurochem Res* **41**, 130-143 (2016). https://doi.org/10.1007/s11064-015-1747-2

7 Chrast, R., Saher, G., Nave, K.-A. & Verheijen, M. H. G. Lipid metabolism in myelinating glial cells: lessons from human inherited disorders and mouse models. *Journal of Lipid Research* **52**, 419-434 (2011). https://doi.org/10.1194/jlr.R009761

8 Ryan, C. B., Choi, J. S., Al-Ali, H. & Lee, J. K. Myelin and non-myelin debris contribute to foamy macrophage formation after spinal cord injury. *Neurobiology of Disease* **163**, 105608 (2022). https://doi.org/https://doi.org/10.1016/j.nbd.2021.105608

9 Haidar, M. *et al.* Targeting lipophagy in macrophages improves repair in multiple sclerosis. *Autophagy* **18**, 2697-2710 (2022). https://doi.org/10.1080/15548627.2022.2047343

10 Peter, M. *et al.* Cerebrospinal fluid lipidomic biomarker signatures of demyelination for multiple sclerosis and Guillain-Barre syndrome. *Sci Rep* **10**, 18380 (2020). https://doi.org/10.1038/s41598-020-75502-x

11 Nogueras, L. *et al.* Lipid profile of cerebrospinal fluid in multiple sclerosis patients: a potential tool for diagnosis. *Sci Rep* **9**, 11313 (2019). https://doi.org/10.1038/s41598-019-47906-x

12 Eckhardt, M. The role and metabolism of sulfatide in the nervous system. *Mol Neurobiol* **37**, 93-103 (2008). https://doi.org/10.1007/s12035-008-8022-3

13 Thudichum, J. L. W. A Treastise on the Chemical Constitution of the Brain: based throughout upon Original Researches. *Glasg. Med. J.* **22**, 363-364 (1884).

14 Blomqvist, M., Zetterberg, H., Blennow, K. & Mansson, J. E. Sulfatide in health and disease. The evaluation of sulfatide in cerebrospinal fluid as a possible biomarker for neurodegeneration. *Mol Cell Neurosci* **116**, 103670 (2021). https://doi.org/10.1016/j.mcn.2021.103670

15 Takahashi, T. & Suzuki, T. Role of sulfatide in normal and pathological cells and tissues. *J Lipid Res* **53**, 1437-1450 (2012). https://doi.org/10.1194/jlr.R026682

16 Hirahara, Y. *et al.* Sulfatide species with various fatty acid chains in oligodendrocytes at different developmental stages determined by imaging mass spectrometry. *J Neurochem* **140**, 435-450 (2017). https://doi.org/10.1111/jnc.13897

17 Honke, K. Biosynthesis and biological function of sulfoglycolipids. *Proc Jpn Acad Ser B Phys Biol Sci* **89**, 129-138 (2013). https://doi.org/10.2183/pjab.89.129

18 Tracey, T. J., Steyn, F. J., Wolvetang, E. J. & Ngo, S. T. Neuronal Lipid Metabolism: Multiple Pathways Driving Functional Outcomes in Health and Disease. *Front Mol Neurosci* **11**, 10 (2018). https://doi.org/10.3389/fnmol.2018.00010

19 Kaya, I. *et al.* Delineating Amyloid Plaque Associated Neuronal Sphingolipids in Transgenic Alzheimer's Disease Mice (tgArcSwe) Using MALDI Imaging Mass Spectrometry. *ACS Chem Neurosci* **8**, 347-355 (2017). https://doi.org/10.1021/acschemneuro.6b00391

20 Magnusson, R. *et al.* RNA-sequencing and mass-spectrometry proteomic time-series analysis of T-cell differentiation identified multiple splice variants models that predicted validated protein biomarkers in inflammatory diseases. *Front Mol Biosci* **9**, 916128 (2022). https://doi.org/10.3389/fmolb.2022.916128

21 Liu, H. *et al.* Label-free Quantitative Proteomic Analysis of Cerebrospinal Fluid and Serum in Patients With Relapse-Remitting Multiple Sclerosis. *Front Genet* **13**, 892491 (2022). https://doi.org/10.3389/fgene.2022.892491

22 Huang, J. *et al.* Inflammation-related plasma and CSF biomarkers for multiple sclerosis. *Proc Natl Acad Sci U S A* **117**, 12952-12960 (2020). https://doi.org/10.1073/pnas.1912839117

23 Chase Huizar, C., Raphael, I. & Forsthuber, T. G. Genomic, proteomic, and systems biology approaches in biomarker discovery for multiple sclerosis. *Cell Immunol* **358**, 104219 (2020). https://doi.org/10.1016/j.cellimm.2020.104219

24 Ziemssen, T., Akgun, K. & Bruck, W. Molecular biomarkers in multiple sclerosis. *J Neuroinflammation* **16**, 272 (2019). https://doi.org/10.1186/s12974-019-1674-2

25 Avasarala, J. R., Wall, M. R. & Wolfe, G. M. A distinctive molecular signature of multiple sclerosis derived from MALDI-TOF/MS and serum proteomic pattern analysis: detection of three biomarkers. *J Mol Neurosci* **25**, 119-125 (2005). https://doi.org/10.1385/JMN:25:1:119

26 Westman, A., Nilsson, C. L. & Ekman, R. Matrix-assisted laser desorption/ionization time-of-flight mass spectrometry analysis of proteins in human cerebrospinal fluid. *Rapid Commun Mass Spectrom* **12**, 1092-1098 (1998). https://doi.org/10.1002/(SICI)1097-0231(19980831)12:16<1092::AID-RCM286>3.0.CO;2-N

27 Cerruti, C. D., Benabdellah, F., Laprevote, O., Touboul, D. & Brunelle, A. MALDI imaging and structural analysis of rat brain lipid negative ions with 9-aminoacridine matrix. *Anal Chem* **84**, 2164-2171 (2012). https://doi.org/10.1021/ac2025317

28 Yang, E., Dufresne, M. & Chaurand, P. Enhancing ganglioside species detection for MALDI-TOF imaging mass spectrometry in negative reflectron mode. *International Journal of Mass Spectrometry* **437**, 3-9 (2019). https://doi.org/https://doi.org/10.1016/j.ijms.2017.09.011

29 Djambazova, K. V. *et al.* Resolving the Complexity of Spatial Lipidomics Using MALDI TIMS Imaging Mass Spectrometry. *Anal Chem* **92**, 13290-13297 (2020). https://doi.org/10.1021/acs.analchem.0c02520

30 Miyawaki, S. *et al.* Imaging mass spectrometry detects dynamic changes of phosphatidylcholine in rat hippocampal CA1 after transient global ischemia. *Neuroscience* **322**, 66-77 (2016). https://doi.org/10.1016/j.neuroscience.2016.02.013

31 Chen, K., Baluya, D., Tosun, M., Li, F. & Maletic-Savatic, M. Imaging Mass Spectrometry: A New Tool to Assess Molecular Underpinnings of Neurodegeneration. *Metabolites* **9** (2019). https://doi.org/10.3390/metabo9070135

32 Ceuppens, R. *et al.* Direct profiling of myelinated and demyelinated regions in mouse brain by imaging mass spectrometry. *International Journal of Mass Spectrometry* **260**, 185-194 (2007). https://doi.org/https://doi.org/10.1016/j.ijms.2006.09.007

33 Jackson, S. N., Wang, H. Y. & Woods, A. S. Direct profiling of lipid distribution in brain tissue using MALDI-TOFMS. *Anal Chem* **77**, 4523-4527 (2005). https://doi.org/10.1021/ac050276v

34 Bredehoft, J. *et al.* Visualizing and Profiling Lipids in the OVLT of Fat-1 and Wild Type Mouse Brains during LPS-Induced Systemic Inflammation Using AP-SMALDI MSI. *ACS Chem Neurosci* **10**, 4394-4406 (2019). https://doi.org/10.1021/acschemneuro.9b00435

35 Yuki, D. *et al.* Hydroxylated and non-hydroxylated sulfatide are distinctly distributed in the human cerebral cortex. *Neuroscience* **193**, 44-53 (2011). https://doi.org/10.1016/j.neuroscience.2011.07.045

36 Kaya, I. *et al.* Spatial Lipidomics Reveals Region and Long Chain Base Specific Accumulations of Monosialogangliosides in Amyloid Plaques in Familial Alzheimer's Disease Mice (5xFAD) Brain. *ACS Chem Neurosci* **11**, 14-24 (2020). https://doi.org/10.1021/acschemneuro.9b00532

37 Kaya, I. *et al.* Brain region-specific amyloid plaque-associated myelin lipid loss, APOE deposition and disruption of the myelin sheath in familial Alzheimer’s disease mice. *Journal of Neurochemistry* **154**, 84-98 (2020). https://doi.org/https://doi.org/10.1111/jnc.14999

38 Kaya, I. *et al.* Brain-region-specific lipid dysregulation in L-DOPA-induced dyskinesia in a primate model of Parkinson’s disease. *npj Parkinson's Disease* **11**, 258 (2025). https://doi.org/10.1038/s41531-025-01109-6

39 Pathmasiri, K. C. *et al.* Mass spectrometry imaging and LC/MS reveal decreased cerebellar phosphoinositides in Niemann-Pick type C1-null mice. *J Lipid Res* **61**, 1004-1013 (2020). https://doi.org/10.1194/jlr.RA119000606

40 Constantinescu, C. S., Farooqi, N., O'Brien, K. & Gran, B. Experimental autoimmune encephalomyelitis (EAE) as a model for multiple sclerosis (MS). *Br J Pharmacol* **164**, 1079-1106 (2011). https://doi.org/10.1111/j.1476-5381.2011.01302.x

41 Curtis II, D. A. *Experimental autoimmune encephalomyelitis as a model of Multiple Sclerosis : pathogenesis of atypical disease and*

tolerance induction in chronic progressive disease Ph.D. thesis, Eastern Carolina University, (2015).

42 Murphy, R. C. & Axelsen, P. H. Mass spectrometric analysis of long-chain lipids. *Mass Spectrom Rev* **30**, 579-599 (2011). https://doi.org/10.1002/mas.20284

43 Hartler, J., Tharakan, R., Kofeler, H. C., Graham, D. R. & Thallinger, G. G. Bioinformatics tools and challenges in structural analysis of lipidomics MS/MS data. *Brief Bioinform* **14**, 375-390 (2013). https://doi.org/10.1093/bib/bbs030

44 Leopold, J., Popkova, Y., Engel, K. M. & Schiller, J. Recent Developments of Useful MALDI Matrices for the Mass Spectrometric Characterization of Lipids. *Biomolecules* **8** (2018). https://doi.org/10.3390/biom8040173

45 Kyle, J. E. *et al.* Uncovering biologically significant lipid isomers with liquid chromatography, ion mobility spectrometry and mass spectrometry. *Analyst* **141**, 1649-1659 (2016). https://doi.org/10.1039/c5an02062j

46 Kister, A. & Kister, I. Overview of myelin, major myelin lipids, and myelin-associated proteins. *Front Chem* **10**, 1041961 (2022). https://doi.org/10.3389/fchem.2022.1041961

47 Ikeda, K. & Taguchi, R. Highly sensitive localization analysis of gangliosides and sulfatides including structural isomers in mouse cerebellum sections by combination of laser microdissection and hydrophilic interaction liquid chromatography/electrospray ionization mass spectrometry with theoretically expanded multiple reaction monitoring. *Rapid Commun Mass Spectrom* **24**, 2957-2965 (2010). https://doi.org/10.1002/rcm.4716

48 Taylor, C. M., Marta, C. B., Bansal, R. & Pfeiffer, S. E. in *Myelin Biology and Disorders* (eds Robert A. Lazzarini *et al.*) 57-88 (Academic Press, 2004).

49 O'Brien, J. S. & Sampson, E. L. Lipid composition of the normal human brain: gray matter, white matter, and myelin. *J Lipid Res* **6**, 537-544 (1965).

50 Bittner, S., Afzali, A. M., Wiendl, H. & Meuth, S. G. Myelin oligodendrocyte glycoprotein (MOG35-55) induced experimental autoimmune encephalomyelitis (EAE) in C57BL/6 mice. *J Vis Exp* (2014). https://doi.org/10.3791/51275

51 Graulich, D. M., Kaiser, S., Sachser, N. & Richter, S. H. Looking on the bright side of bias—Validation of an affective bias test for laboratory mice. *Applied Animal Behaviour Science* **181**, 173-181 (2016). https://doi.org/https://doi.org/10.1016/j.applanim.2016.05.011

52 Cumming, G., Fidler, F. & Vaux, D. L. Error bars in experimental biology. *J Cell Biol* **177**, 7-11 (2007). https://doi.org/10.1083/jcb.200611141

53 Shin, K. C., Ali Moussa, H. Y. & Park, Y. Cholesterol imbalance and neurotransmission defects in neurodegeneration. *Exp Mol Med* **56**, 1685-1690 (2024). https://doi.org/10.1038/s12276-024-01273-4

54 Quarles, R. H. Myelin sheaths: glycoproteins involved in their formation, maintenance and degeneration. *Cell Mol Life Sci* **59**, 1851-1871 (2002). https://doi.org/10.1007/pl00012510

55 Tobias, F., Pathmasiri, K. C. & Cologna, S. M. Mass spectrometry imaging reveals ganglioside and ceramide localization patterns during cerebellar degeneration in the Npc1(-/-) mouse model. *Anal Bioanal Chem* **411**, 5659-5668 (2019). https://doi.org/10.1007/s00216-019-01989-7

56 Sekera, E. R., Saraswat, D., Zemaitis, K. J., Sim, F. J. & Wood, T. D. MALDI Mass Spectrometry Imaging in a Primary Demyelination Model of Murine Spinal Cord. *J Am Soc Mass Spectrom* **31**, 2462-2468 (2020). https://doi.org/10.1021/jasms.0c00187

57 Stoffel, W. & Bosio, A. Myelin glycolipids and their functions. *Curr Opin Neurobiol* **7**, 654-661 (1997). https://doi.org/10.1016/s0959-4388(97)80085-2

58 Ramakrishnan, H. *et al.* Increasing sulfatide synthesis in myelin-forming cells of arylsulfatase A-deficient mice causes demyelination and neurological symptoms reminiscent of human metachromatic leukodystrophy. *J Neurosci* **27**, 9482-9490 (2007). https://doi.org/10.1523/JNEUROSCI.2287-07.2007

59 Okuda, D. T. Radiologically Isolated Syndrome: MR Imaging Features Suggestive of Multiple Sclerosis Prior to First Symptom Onset. *Neuroimaging Clin N Am* **27**, 267-275 (2017). https://doi.org/10.1016/j.nic.2016.12.008

60 Raphael, I. *et al.* TNFR2 limits proinflammatory astrocyte functions during EAE induced by pathogenic DR2b-restricted T cells. *JCI Insight* **4** (2019). https://doi.org/10.1172/jci.insight.132527

61 Ji, N. *et al.* Small molecule inhibitor of antigen binding and presentation by HLA-DR2b as a therapeutic strategy for the treatment of multiple sclerosis. *J Immunol* **191**, 5074-5084 (2013). https://doi.org/10.4049/jimmunol.1300407

62 Nelson, K. A., Daniels, G. J., Fournie, J. W. & Hemmer, M. J. Optimization of whole-body zebrafish sectioning methods for mass spectrometry imaging. *J Biomol Tech* **24**, 119-127 (2013). https://doi.org/10.7171/jbt.13-2403-002

63 Angel, P. M., Spraggins, J. M., Baldwin, H. S. & Caprioli, R. Enhanced sensitivity for high spatial resolution lipid analysis by negative ion mode matrix assisted laser desorption ionization imaging mass spectrometry. *Anal Chem* **84**, 1557-1564 (2012). https://doi.org/10.1021/ac202383m

64 Yang, J. & Caprioli, R. M. Matrix sublimation/recrystallization for imaging proteins by mass spectrometry at high spatial resolution. *Anal Chem* **83**, 5728-5734 (2011). https://doi.org/10.1021/ac200998a

65 Thomas, A., Charbonneau, J. L., Fournaise, E. & Chaurand, P. Sublimation of new matrix candidates for high spatial resolution imaging mass spectrometry of lipids: enhanced information in both positive and negative polarities after 1,5-diaminonapthalene deposition. *Anal Chem* **84**, 2048-2054 (2012). https://doi.org/10.1021/ac2033547

66 Sladkova, K., Houska, J. & Havel, J. Laser desorption ionization of red phosphorus clusters and their use for mass calibration in time-of-flight mass spectrometry. *Rapid Commun Mass Spectrom* **23**, 3114-3118 (2009). https://doi.org/10.1002/rcm.4230